


RESEARCH ARTICLE

Monomeric/dimeric forms of Fgf15/FGF19 show differential activity in hepatocyte proliferation and metabolic function

Courtney M. Williams  | Jessica Harper Calderon | Hock E | Yasalp Jimenez |
Kevin Barringer | Marisa Carbonaro | Maria del Pilar Molina-Portela |
Gavin Thurston | Zhe Li | Christopher Daly

Oncology and Angiogenesis Department,
Regeneron Pharmaceuticals, Inc.,
Tarrytown, NY, USA

Correspondence

Courtney M. Williams, Oncology and
Angiogenesis Department, Regeneron
Pharmaceuticals, Inc, 777 Old Saw Mill
River Road, Tarrytown, NY 10591, USA.
Email: courtney.williams@regeneron.com

Funding information

Regeneron Pharmaceuticals (Regeneron)

Abstract

Human Fibroblast Growth Factor 19 (FGF19) and mouse ortholog Fgf15 play similar roles in liver regeneration and metabolism via the activation of Fgfr4/b-klotho (Klb). Monomeric FGF19 and dimeric Fgf15 are both necessary for liver regeneration and proper bile acid (BA) metabolism. FGF19 elicits stronger effects than Fgf15 on glucose and fatty acid metabolism and only FGF19 induces hepatocellular carcinoma (HCC). However, inhibiting FGF19/FGFR4 signaling in HCC patients is associated with toxicity due to elevated BA levels. Here, we examine the structure/function relationship in Fgf15/FGF19 to better understand the molecular basis for their distinct functions. We demonstrate that FGF19 is a more effective activator of Fgfr4 and of downstream signaling (Erk, Plcg1) than Fgf15. Furthermore, we use site-directed mutagenesis to show that the presence or absence of an unpaired cysteine in Fgf15/19 modulates ligand structure and determines the ability of these molecules to induce hepatocyte proliferation, with monomers being more potent activators. Consistent with these findings, an engineered dimeric variant of FGF19 is less effective than wild-type FGF19 at inducing liver growth in cooperation with the Wnt-enhancer RSPO3. In contrast to effects on proliferation, monomeric and dimeric ligands equally inhibited the expression of *Cyp7a1*, the enzyme catalyzing the rate limiting step in BA production. Thus, structure and function of Fgf15/FGF19 are intricately linked, explaining why FGF19, but not Fgf15, induces liver tumorigenesis. Our data provide insight into FGF19/FGFR4 signaling and may inform strategies to target this pathway while limiting on-target toxicity due to dysregulation of BA production or induction of hepatocyte proliferation.

KEYWORDS

bile, carcinogenesis, FGFR4 protein, FGF19 protein, hepatocytes, hepatocellular carcinoma, liver regeneration, structure-activity relationship

Abbreviations: BA, Bile Acids; DAPI, 4'-6-diamidino-2-phenylindole; FGF, fibroblast growth factor; FGFR, fibroblast growth factor receptor; HCC, hepatocellular carcinoma; HDD, hydrodynamic delivery; IHC, immunohistochemistry; NASH, nonalcoholic steatohepatitis; PCR, polymerase chain reaction; PSC, primary sclerosing cholangitis.

This is an open access article under the terms of the Creative Commons Attribution-NonCommercial License, which permits use, distribution and reproduction in any medium, provided the original work is properly cited and is not used for commercial purposes.

© 2021 Regeneron Pharmaceuticals, Inc. *The FASEB Journal* published by Wiley Periodicals, Inc. on behalf of Federation of American Societies for Experimental Biology

1 | INTRODUCTION

Human FGF19 and its mouse ortholog Fgf15 are enterocrine FGFs that share 51% amino acid identity¹ and function to regulate BA synthesis.² These atypical FGFs act distant to their site of production and require Klb as a co-receptor for Fgfr4 signaling. In a negative feedback loop, BA produced in the liver stimulates enterocytes of the ileum to produce Fgf15/FGF19, which circulate to the liver and inhibit hepatocyte expression of *Cyp7a1*, the enzyme that catalyzes the rate limiting step in BA synthesis. Fgf15 is also known to be crucial for liver regeneration after partial hepatectomy, with *Fgf15* knockout mice showing high mortality.³

While many studies have used Fgf15 and FGF19 interchangeably, these proteins are not as closely related as other FGF homologs (51% identity for Fgf15 and FGF19, vs 81%-99% for FGF1-8).⁴ Although both equally regulate BA production, FGF19 is a more potent regulator of blood glucose, lipid metabolism and body weight in certain mouse backgrounds.² Furthermore, FGF19 overexpression induces HCC in genetically engineered mouse models^{2,5-7} and FGF19 genetic amplification drives a subset of HCC,⁸ a potential tradeoff that comes with more potent metabolic signaling. While Fgf15 has been reported to play a role in promoting fibrosis-associated HCC development,⁹ Fgf15 does not induce HCC when overexpressed in mice.²

Due to its role in HCC and BA production, the FGF19/FGFR4 pathway is an attractive therapeutic target. However, attempts to inhibit FGF19/FGFR4 signaling in HCC are complicated by on-target toxicity in liver and gut due to dysregulated expression of *Cyp7a1* and overproduction of BA.^{10,11} Pathway activation to treat metabolic disorders (eg, NASH) could potentially induce hepatocyte proliferation, thereby increasing cancer risk. In an attempt to address this, a variant of FGF19, known as M70, was created through the introduction of several N-terminal mutations.^{6,12} M70 retains the ability to regulate BA production, but unlike wild-type FGF19, fails to drive liver tumorigenesis in mouse models. This agent has shown efficacy in preclinical models of cholestatic liver disease and is currently being evaluated clinically (known as NGM282 or aldafermin in the clinic) for the treatment of NASH.¹³⁻¹⁶

While the molecular basis of the functional differences between Fgf15 and FGF19 remains unclear, Zhou et al showed that Fgf15 circulates as a dimer, whereas FGF19 is monomeric.² The authors speculate about, but do not directly prove, that this structural difference is due to the presence of an unpaired cysteine in Fgf15. However, the study does not directly assess the role of this cysteine residue in FGF15/19 structure/function nor does it examine in detail the signal transduction pathways that are activated by these two ligands. Thus, it remains unclear whether the different biological effects of Fgf15/FGF19 are due to activation of distinct downstream signaling pathways or simply reflect a difference in ligand potency.

In this report, we show that the presence or absence of an unpaired cysteine in Fgf15/19 modulates ligand structure (monomer vs dimer) and determines the ability of these molecules to induce hepatocyte proliferation as single agents in vitro, and in combination with the Wnt enhancer RSPO3 in vivo. In contrast, monomeric and dimeric Fgf15/FGF19 are equally capable of regulating BA production. Together, our data indicate that the structure and function of Fgf15/FGF19 are intricately linked and explain why FGF19, but not Fgf15, induces liver tumorigenesis. Our findings help to elucidate the molecular basis for the distinct biological effects of Fgf15/FGF19 and to inform strategies for safe and effective therapeutic targeting of the FGF19/FGFR4 pathway.

2 | MATERIALS AND METHODS

2.1 | Animal care

All animal studies were approved and performed in accordance the Institutional Animal Care and Use Committee (IACUC) guidelines at Regeneron Pharmaceuticals, Inc and in compliance with the US National Research Council's Guide for the Care and Use of Laboratory Animals, the US Public Health Service's Policy on Humane Care and Use of Laboratory Animals, and Guide for the Care and Use of Laboratory Animals. Mice were housed in a pathogen-free animal facility under a controlled light/dark cycle and fed a standard chow diet with access to autoclaved water. All experimentation on mice was performed during the light cycle. Upon sacrifice, mice were euthanized by carbon dioxide and cervical dislocation. All studies conform to the Animal Research: Reporting of In Vivo Experiments (ARRIVE) guidelines.

2.2 | In vivo experiments

For hydrodynamic delivery (HDD), 25-50 µg/mouse of plasmid coding for *Fgf15* (GenBank: NM_008003.2), *Fgf15*^{C135P}, *FGF19* (GenBank: NM_005117.3), *FGF19*^{P128C}, human Fc, or 0.5 µg/mouse *Il6* plasmid were diluted in sterile saline (0.9% NaCl) to a volume approximately 10% of body weight and injected into the tail vein of 6- to 12-week-old male or female Taconic C.B-Igh-1b/ICR-*Prkdc*^{scid} mice (Taconic Biosciences, Rensselaer, NY, USA).¹⁷ Animals were only excluded from analysis if they failed to express HDD constructs.

Where indicated, mice were pre-dosed via intraperitoneal injection with 25 mg/kg of either control (hFc) or Il6r blocking antibodies 24 hours prior to HDD. Antibodies were generated in-house (Zhang, L 2017, *Methods of inhibiting tumor growth by antagonizing IL-6 receptor*, United States patent US 9,409,990 B2; Stevens, S, Huan, TT, Martin, JH, Fairhurst, JL, Rafique, A, Smith, E, Pobursky, KJ, Papadopoulos, NJ, Fandl, JP, Chen, G, Karow, M 2009, *High*

affinity antibodies to human IL-6 receptor, United States patent US 7,582,298 B2.)

2.3 | Cell culture

Hek293T (ATCC CRL-3216 RRID:CVCL_0063) and AML12 cells (ATCC CRL-2254 RRID:CVCL_0140)¹⁸ were cultured per ATCC protocol. STR profile testing was performed on Hek293T, October 2012, AML12, July 2020 (ATCC, Manassas, VA, USA). To produce conditioned media, Hek293T cells were seeded at 200 000 cells/well in 6-well plates and transfected with 2.5 µg/µL of the plasmids used for HDD according to the manufacturer's protocol for Lipofectamine 3000 (Thermo Fisher Scientific, Waltham, MA, USA). Media was changed to serum-free media 72 hours post-transfection and media was collected 24 hours later and combined with an equal amount of Opti-MEM (Thermo Fisher Scientific, Waltham, MA, USA).

FGF19^{P128C} conditioned medium was concentrated with Amicon Ultra-0.5 centrifugal filter (UFC501008, Millipore Sigma, Burlington, MA, USA) according to the manufacturer's protocol. Conditioned media and recombinant FGF19 (969-FG-025, R&D Systems, Minneapolis, MN, USA) were separated by SDS-PAGE and proteins were visualized with Pierce Silver Stain kit (24612, Thermo Fisher Scientific, Waltham, MA, USA). Serum (0.5 µL) from mice receiving HDD constructs was combined with either reducing or non-reducing 2X Laemmli SDS sample buffer and proteins were separated by SDS-PAGE. Fgf15 antibody (LS-B15011, LS Bio, Seattle, WA, USA, RRID:AB_2868448) was used at 1 µg/mL in 5% milk. FGF19 antibody (AF969, RRID:AB_355750, R&D Systems, Minneapolis, MN, USA) was used at 0.5 µg/mL in 5% milk.

2.4 | Cell proliferation assay

AML12 cells were seeded in a 24-well plate in DMEM supplemented with 2% of FBS, 2 mM of L-Glutamine, and 1× of penicillin-streptomycin (Pen Strep Glutamine 100X) (10378-016 Gibco, Gaithersburg, MD, USA). Polycarbonate tissue culture-treated inserts with a 0.4 µm pore size were inserted in each well. Untransfected Hek293T cells supplemented with recombinant human FGF19 (969-FG-025, R&D systems, Minneapolis, MN, USA) and Hek293T cells 72 hours post-transfection were also seeded in inserts. After 1 day and 6 days in culture, viable cell number was measured using CellTiter 96 AQueous One Solution Cell Proliferation Assay (MTS) (Promega, Madison, WI, USA) as per the manufacturer's protocol. Absorbance at 490 nm was read on SpectraMax M3 plate reader (Molecular Devices, San Jose, CA, USA). Percent increase in growth was determined by normalizing absorbance at 6 days to day 1 in culture. The FGFR1-3 inhibitor AZD4547 (S2801, Selleckchem, Houston, TX, USA) was used at 30 nM

and the FGFR4 inhibitor BLU9931 was used at 10 nM (538776, Sigma Aldrich, St. Louis, MO, USA), replaced on Day 3.

2.5 | Immunoprecipitation and western blotting

Protein lysates from cells were extracted in cold RIPA Lysis and Extraction Buffer combined with 1X Halt Protease and Phosphatase Inhibitor Cocktail (Thermo Fisher Scientific, Waltham, MA, USA). Protein lysates from liver tissue were extracted from frozen liver tissue samples homogenized with ice-cold homogenization buffer consisting of NaCl 150 mM, Tris, pH 7.5 20 mM, Triton X 1%, and 1X Halt Protease and Phosphatase Inhibitor Cocktail (Thermo Fisher Scientific, Waltham, MA, USA). Tissue was homogenized thrice, in 10 second intervals, on ice. Protein quantification was determined by bicinchoninic acid assay (BCA) assay (5000002, Bio-Rad, Hercules, CA, USA) and lysate was combined with reducing 2X Laemmli SDS sample buffer and ran on a Novex™ 4%-12% Tris Glycine gel (Invitrogen, Carlsbad, CA).

Antibodies used for Western blotting are Phospho-p44/42 MAPK (Erk1/2) (4370, RRID:AB_2315112), p44/42 MAPK (Erk 1/2) (9102, RRID:AB_330744), Phospho-Plcg1 (14008, RRID:AB_2728690), Plcg1 (2822, RRID:AB_2163702), S6 ribosomal protein (2217, RRID:AB_331355), and phospho-S6 (Ser 235/236) (4858, RRID:AB_916156) antibodies (Cell Signaling, Danvers, MA, USA) were used at 1:500 in 5% milk. Phospho-Frs2 (R&D Systems AF5126, RRID:AB_2106234, Minneapolis, MN, USA) was used at 2 µg/mL in PBST. Abcam Frs2 (ab200548, RRID:AB_2747582, Abcam, Cambridge, UK) was used at 0.5 µg/mL in PBST. Fgf15 antibody (LS-B15011, LS Bio, Seattle, WA, USA, RRID:AB_2868448) was used at 1 µg/mL in 5% milk. FGF19 antibody (AF969, RRID:AB_355750, R&D Systems, Minneapolis, MN, USA) was used at 0.5 µg/mL in 5% milk.

For immunoprecipitation lysates were precleared with Protein A/G PLUS-Agarose beads (sc-2003, RRID:AB_10201400, Santa Cruz Biotechnology Dallas, TX, USA) then immunocomplexes were precipitated with Anti-phosphotyrosine 4G10 platinum agarose conjugate beads (Millipore 16-638, RRID:AB_11212502, Millipore Sigma, Burlington, MA, USA). Primary antibody against Fgfr4 (8562, RRID:AB_10891199, Cell Signaling, Danvers, MA, USA) was used at 1:500 in 5% milk. Cell lysate prior to immunoprecipitation was probed with anti-β-Actin antibody (Sigma A5316, RRID:AB_476743, Millipore Sigma, Burlington, MA, USA) used at 1:2000 in 5% milk.

TaqMan Tissues were homogenized in TRIzol and purified using MagMAX-96 for Microarrays Total RNA Isolation Kit (Ambion by Life Technologies, Carlsbad, CA, USA) according to the manufacturer's specifications. Genomic DNA was removed using RNase-Free DNase Set (Qiagen, Hilden, Germany).

mRNA was reverse-transcribed into cDNA using SuperScript VILO Master Mix (Invitrogen Life Technologies, Carlsbad, CA) and Veriti 96-well PCR Thermal Cycler (Thermo Fisher Scientific, Waltham, MA, USA). cDNA was amplified with SensiFAST Probe Hi-ROX (Meridian Life Science, Memphis, TN, USA) using 12k Flex System (Applied Biosystems, Foster City, CA). PCR reactions done in triplicate. Beta-actin was used to normalize cDNA input differences. Data reported as comparative CT method using delta delta CT. Probes described in Supporting Informations and methods.

2.6 | Serum chemistry

Assays are performed on Siemens ADVIA Chemistry XPT (Siemens, Munich, Germany). Analyses use the following reagents following the manufacturer guidelines Alanine Aminotransferase (ALT)—(Siemens REF 03036926), Aspartate Aminotransferase (AST)—(Siemens REF 07499718), Cholesterol₂ (CHOL₂)—(Siemens REF 10376501), Direct HDL Cholesterol (D-HDL)—(Siemens REF 07511947), LDL Cholesterol Direct (DLDL)—(Siemens REF 09793248), Non-Esterified Fatty Acids (NEFA)—(Wako 999-34691, 995-34791, 991-34891, 993-35191, Wako Diagnostics, Mountain View, CA), Triglycerides₂ (TRIG₂)—(Siemens REF 10335892), Glucose₂ Hexokinase₃ (GLUH₃)—(Siemens REF 05001429), Beta Hydroxy Butyrate (BHOB)—(StanBio Laboratory REF 2440-058, EKF Diagnostics, Boerne, TX, USA), and Total Bile Acids (TBA)—(Diazyme REF DZ042A, Diazyme Laboratories, Poway, CA). Each set of reagents is calibrated as recommended by the manufacturer and samples with known values (Multilevel Quality Controls) are measured daily.

2.7 | Statistical analysis

All statistical analyses were performed in GraphPad Prism (RRID:SCR_002798) using ANOVA with Tukey's multiple comparisons test. Sample numbers are specified in figure legends.

2.8 | Immunohistochemistry

Mouse liver tissues were fixed in 4% paraformaldehyde and dehydrated in 70% Ethanol. Tissue processing, paraffin wax embedding, tissue sectioning, and subsequent staining for hematoxylin and eosin (H&E) or antibodies against Ki-67 (Abcam 16667, RRID:AB_302459, Cambridge, UK), Cyp7a1 (Sigma Aldrich MABD42, RRID:AB_2756360,

Millipore Sigma, Burlington, MA, USA), and Glutamine Synthetase (Abcam 73593, RRID:AB_2247588, Cambridge, UK) were conducted by HistoServ (Germantown, MD). Slides were scanned on a Leica Aperio AT2 scanner using Aperio eSlide Manager V12.3.3.5049 (Leica Biosystems, Wetzlar, Germany). Images were quantified in HALO Link using the CytoNuclear v1.6 analysis (RRID:SCR_018350, Indica Labs, Corrales, NM, USA). A minimum of two sections per sample were quantified.

2.9 | Immunofluorescence

Samples were prepared as previously described¹⁹ with antibodies Fgfr4 (Santa Cruz sc-136988 1:50, RRID:AB_2103663, Santa Cruz Biotechnology Dallas, TX, USA), Collagen IV (Abcam ab6586 1:100, RRID:AB_305584, Cambridge, UK), Cy3 Donkey Anti-Rabbit (711166152, RRID:AB_2313568), and Alexa Fluor 488 Goat Anti-Mouse (115546062, RRID:AB_2338863) (Jackson Immuno Research Labs 1:200, West Grove, PA). DAPI at 1:250 (Invitrogen D1306, RRID:AB_2629482, Life Technologies, Carlsbad, CA, USA). Sections imaged on a ZEISS LSM780 Confocal laser scanning microscope system with GaAsP detector, alpha Plan-Apochromat 100X/1.46 Oil DIC M27, or Plan-Apochromat 20x/0.8 M27 at room temperature. Images were processed using Zen Black (RRID:SCR_018163, Carl Zeiss AG, Oberkochen, Germany).

3 | RESULTS

3.1 | Structural basis of functional differences between Fgf15 and FGF19

Although there are documented differences between Fgf15 and FGF19 function, potential differences in the activation of intracellular signaling pathways by these ligands have not been characterized. We assessed signaling in the mouse hepatocyte cell line AML12, as mouse Fgfr4/Klb binds to both mouse Fgf15 and human FGF19. Conditioned medium from Hek293T cells expressing FGF19 or Fgf15 was used as a source of these ligands since active recombinant Fgf15 is not commercially available. As shown in Figure 1A, FGF19 is more effective than Fgf15 at promoting phosphorylation of Frs2 (a proximal signaling adaptor for the FGFR family) and of Erk and Plcg1, key drivers for proliferation induced by receptor tyrosine kinases. FGF19 is also a more potent activator of mTOR signaling as measured by phosphorylation of S6 ribosomal protein (Figure S1). Neither FGF19 nor Fgf15 significantly activated the Akt, Stat3, or Gsk3b pathways (data not shown). Since amounts of Fgf15/FGF19 in culture were saturating (~250 ng/mL or 11.5 nM—Figures S2A,B), these

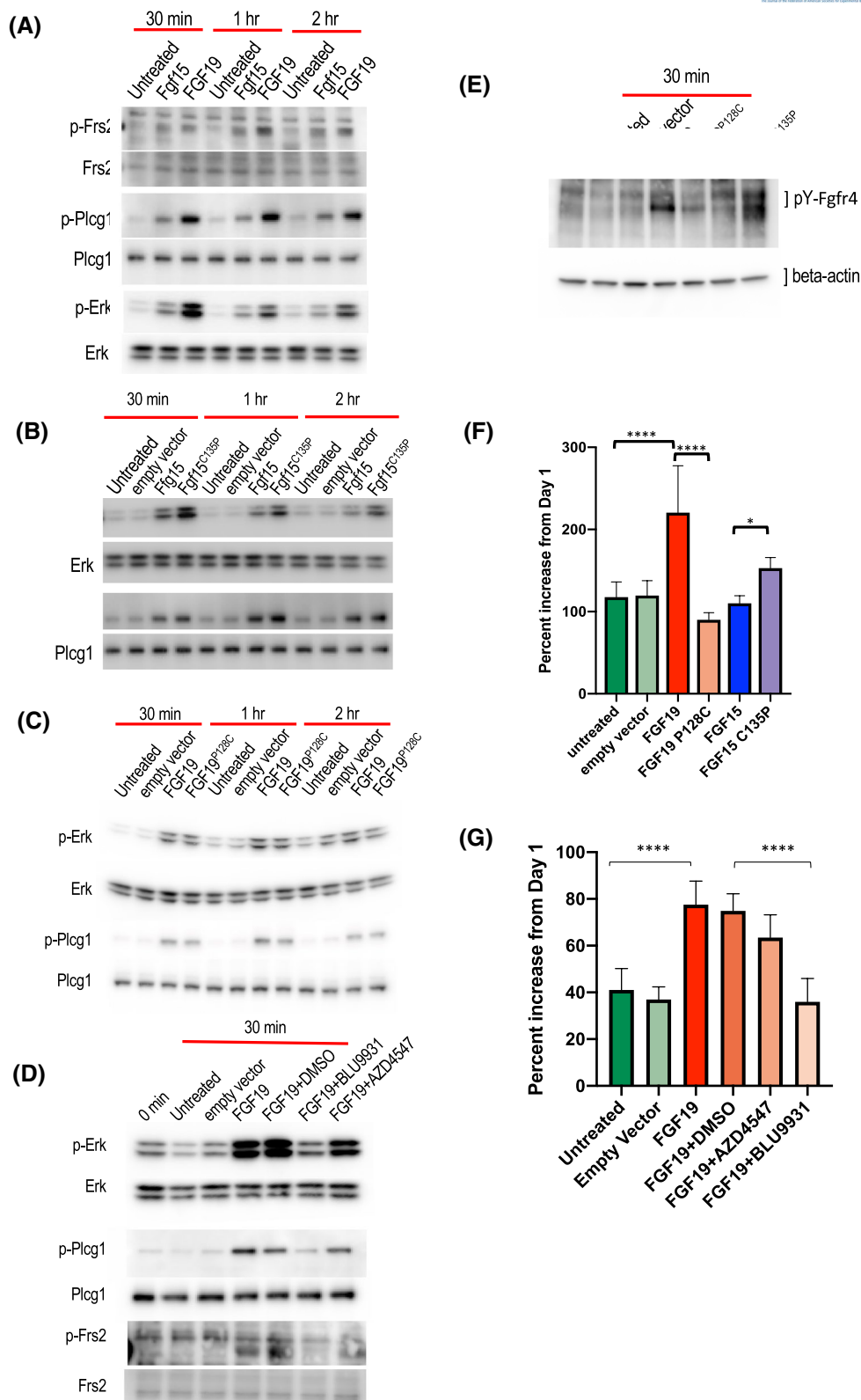


FIGURE 1 Divergent Fgf15/FGF19 structures underlie differential ligand activity. A-D, Western blots of cell lysates from AML12 cells serum-starved overnight and treated for the indicated times with conditioned medium from Hek293T cells expressing the indicated proteins or empty vector control (1:10 dilution of conditioned media for A and B; 1:5 dilution for C). In panel (D), FGFR1-3 inhibitor AZD4547 was used at 30 nM and FGFR4 inhibitor BLU9931 was used at 10 nM. E, AML12 cells were serum-starved overnight then treated for 30 minutes with 1:10 dilution of conditioned medium. Cell lysates were immunoprecipitated with phospho-tyrosine antibody and FGFR4 was detected by Western blot. Equal loading was determined by Western blot of beta-actin in pre-cleared lysate. F, Growth assay of AML12 cells co-cultured with Hek293T cells expressing the indicated proteins (or empty vector control) for 6 days. Bar graph shows the percent increase in cell number after 6 days (mean \pm standard deviation, $n = 8$). G, Same as F, but with 30 nM AZD4547 and 10 nM BLU9931 as indicated. (* $P < .05$; **** $P < .0001$ using ANOVA with Tukey's multiple comparisons test).

results reveal a true difference in ligand efficacy (maximum effect) and not simply a difference in potency. Thus, it appears that the primary difference between Fgf15 and FGF19 with respect to Fgfr4 signaling is the overall strength of pathway activation, rather than the activation of a distinct set of downstream pathways.

Previous reports have speculated that signaling differences between Fgf15 and FGF19 are due to the presence of an unpaired cysteine in Fgf15 that confers the ability to homodimerize. To test this, site-directed mutagenesis was used to remove the unpaired cysteine at position 135 of Fgf15 and to introduce an unpaired cysteine at position 128 of FGF19. Constructs were expressed in Hek293T cells, and proteins in conditioned media were resolved by SDS-PAGE under reducing or non-reducing conditions. As shown in Figure S2C, Fgf15^{C135P} is monomeric in conditioned medium and wild-type Fgf15 is dimeric. The difference between FGF19 and FGF19^{P128C} is less apparent as non-reducing conditions show a weaker band for FGF19 monomer and stronger dimer and trimer bands. The reducing gel shows equivalent amounts of FGF19 and FGF19^{P128C}, indicating that the difference in monomer bands under non-reducing conditions is due to the formation of dimers and/or higher order multimers (Figure S2C). These results demonstrate that the unpaired cysteine is necessary for dimer formation by Fgf15 and that introduction of this cysteine into FGF19 promotes dimer/multimer formation, although not very efficiently in conditioned medium.

To determine whether these mutations and the associated structural changes in Fgf15 and FGF19 alter their signaling properties, AML12 cells were serum-starved overnight and then, stimulated with conditioned media containing the ligands. Monomeric Fgf15^{C135P}-induced phosphorylation of Erk, Plcg1 and S6 ribosomal protein more strongly than wild-type Fgf15 (Figures 1B and S1), despite lower levels of protein in the Fgf15^{C135P} conditioned media (Figure S2D). We observed only minor decreases in Erk and Plcg1 phosphorylation when AML12 cells were treated with FGF19^{P128C} vs wild-type FGF19 (Figure 1C), likely due to the incomplete conversion of FGF19^{P128C} to dimeric/multimeric forms (Figure S2C). To determine whether FGF19/Fgf15 signal through Fgfr4 specifically, we utilized FGFR4 inhibitor BLU9931 and FGFR1-3 inhibitor AZD4547. Only the FGFR4 inhibitor was able to block phosphorylation of Erk and Plcg1 in AML12 cells (Figure 1D). This result is in keeping with analysis of AML12 mRNA expression showing Fgfr4 is the only FGFR expressed in this cell line (data not shown). To assess activation of Fgfr4 itself, AML12 cells were stimulated with conditioned media (Figure S2D,E) for 30 minutes followed by anti-phosphotyrosine immunoprecipitation and Western blot for Fgfr4. FGF19 was a more effective activator of Fgfr4 phosphorylation than Fgf15 (Figure 1E) and the level

of Fgfr4 phosphorylation correlated with the propensity of the ligand to be monomeric (ie, FGF19 > FGF19^{P128C} and Fgf15^{C135P} > Fgf15). Together, these findings suggest that monomerization significantly increases the ability of Fgf15 to activate signaling.

To test whether differences in structure and signaling strength correlate with the ability of these ligands to stimulate proliferation, Hek293T cells expressing the various ligands were co-cultured in a transwell system with AML12 cells for 6 days. As shown in Figure 1F, FGF19 but not FGF19^{P128C} promoted significant cell growth. Fgf15^{C135P} significantly increased proliferation compared to wild-type Fgf15. Fgf15^{C135P} was present in conditioned medium at a lower level than wild-type Fgf15 (Figure S2D), further highlighting the increased activity of monomeric Fgf15. As with signaling, the growth stimulatory effects of FGF19 required Fgfr4 (Figure 1G). Collectively, these data show that the structure of Fgf15/FGF19 directly influences biologic function, with ligand monomers capable of inducing hepatocyte proliferation.

3.2 | Fgf15/FGF19 mutants are biologically active in vivo

To confirm that mutant FGF19 and Fgf15 are functional in vivo, mice were injected with expression constructs via HDD and serum and tissue samples were collected for analysis of protein levels and biological activity. HDD achieved high expression of proteins in serum, for example, FGF19 was present at >1 mg/mL (Figure S3A). Examination of liver microarchitecture by confocal microscopy and three-dimensional reconstruction showed no significant changes at 2 weeks post-HDD (Figure S3B). In serum, Fgf15 was dimeric and Fgf15^{C135P} monomeric (Figure 2A). In contrast, FGF19 was monomeric while the FGF19^{P128C} mutant circulated as a series of higher-order multimers, with little monomer present in serum (Figure 2A). These structural differences are much clearer than was seen in conditioned media in vitro.

In liver lysates collected 1 week after HDD, monomeric Fgf15^{C135P}-induced stronger activation of Plcg1, Erk, and S6 ribosomal protein than wild-type Fgf15, despite lower protein levels in serum, confirming our in vitro finding that Fgf15^{C135P} is a more effective ligand (Figure 2B). In addition, dimeric/multimeric FGF19^{P128C}-induced weaker Plcg1 and S6 activation than wild-type FGF19, although no difference in Erk activation was observed between wild-type and mutant FGF19. Taken together, these data support the contention that the structure of Fgf15/FGF19 ligands controls signaling strength in vivo.

A major function of Fgf15/FGF19 is to signal via FGFR4/KLB to repress expression of *Cyp7a1*, the enzyme that

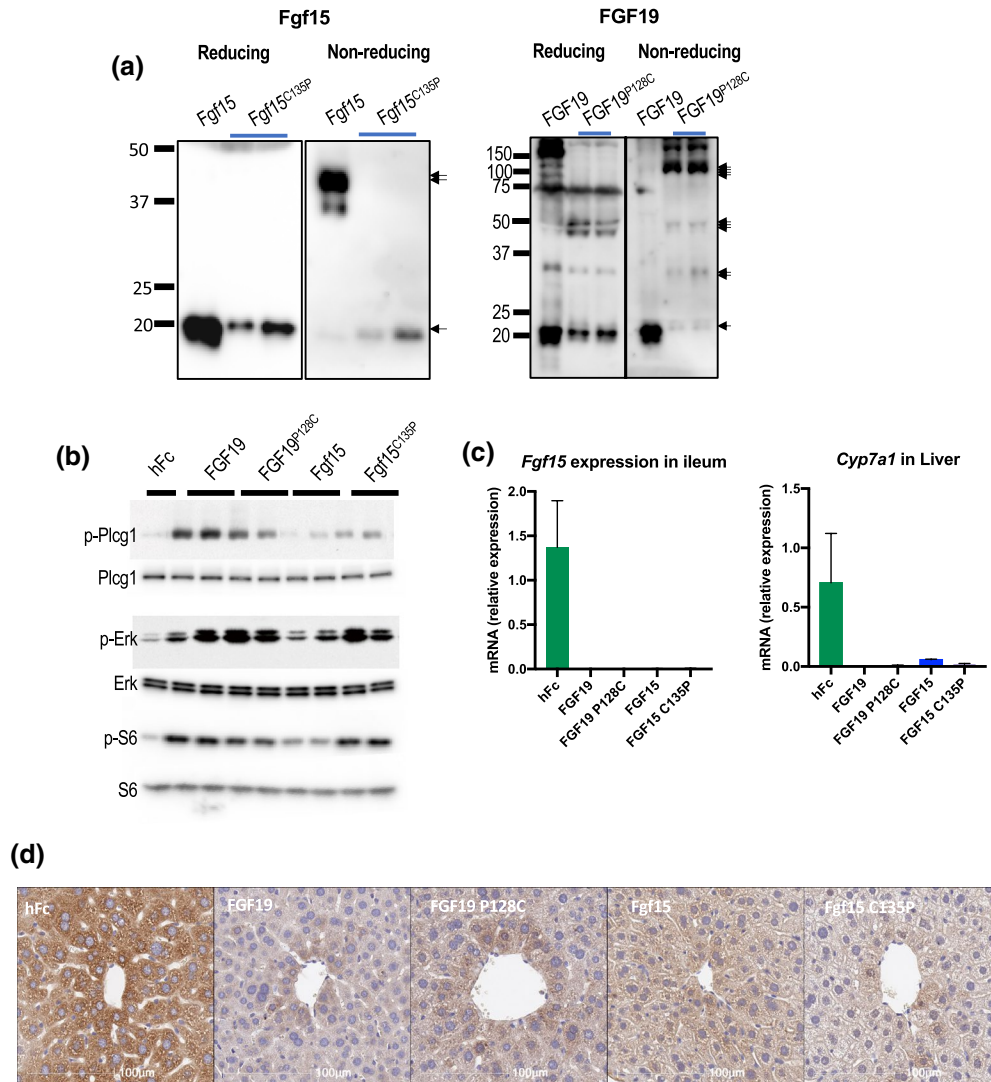


FIGURE 2 FGF15^{C135P} and FGF19^{P128C} are biologically active. A, Reducing and non-reducing Western blots for FGF19 or Fgf15 of sera from male mice 2 weeks after HDD with 25 μ g/mouse of plasmid encoding wild-type FGF15, FGF15^{C135P}, wild-type FGF19, or FGF19^{P128C} via HDD. B, Western blot of liver lysate from male mice treated as in A, but sacrificed at 1 week post-HDD. C, mRNA levels of *Cyp7a1* (liver) or *Fgf15* (ileum) from male mice at 1 week post-HDD. Bar graph depicts the relative mRNA levels vs the empty vector control group (assigned a value of 1.0). Mean \pm standard deviation, $n = 4$ for hFc control, and $n = 5$ for the treatments. PCR reactions were done in triplicate, normalized to beta-actin. D, IHC with Cyp7a1 antibody from mice treated as in A. 40 \times .

catalyzes the rate-limiting step of BA synthesis, in hepatocytes. In turn, BAs stimulate Fgf15 expression in the ileum, setting up the negative feedback loop that controls BA levels. Despite the structural differences in serum and the signaling differences in hepatocytes, Fgf15, Fgf15^{C135P}, FGF19, and FGF19^{P128C} were equally capable of inhibiting *Cyp7a1* expression in liver and endogenous *Fgf15* expression in ileum (Figure 2C). In addition, IHC on liver sections showed that Cyp7a1 protein levels were dramatically lower in mice exposed to any of the ligands compared to the control mice (Figure 2D). These findings suggest that the *Cyp7a1* promoter is very sensitive to Fgfr4 pathway activation, and both wild-type and mutant ligands are able to signal via FGFR4 to repress its expression.

3.3 | FGF19 can synergize with RSPO3 to induce hepatomegaly

Next, we further compared the *in vivo* activity of Fgf15/FGF19 and the variants. Multiple studies have reported that overexpression of FGF19 can induce hepatomegaly.^{2,5,6,20} However, in SCID mice, we did not observe changes in liver size 2 weeks post-HDD of FGF19. Given that Fgfr4/Klb are expressed in Zone 3 of the liver, where Wnt signaling is high (Figure S4), we hypothesized that treatment with Wnt enhancer RSPO3 might expand the number of hepatocytes competent to respond to FGF19 and elicit a growth response. Previous work in our lab has shown that delivery of RSPO3 by HDD is able to induce a rapid, prolonged, dose-dependent

increase in liver size that is associated with an expansion of Zone 3 marker expression (Figure S5).

To test if the combination of enhanced Wnt signaling and activation of Fgfr4/Klb could induce liver growth, we expressed RSPO3 alone or in combination with Fgf15 or FGF19. At 2 weeks post-HDD, we observed that FGF19 enhanced RSPO3-induced liver growth, while Fgf15 had no effect (Figure 3A). Immunohistochemistry for proliferation marker Ki-67 showed increased proliferation in the RSPO3 and the FGF19 + RSPO3-treated livers (Figure S6A,B). Fgf15 did not induce hepatocyte proliferation alone, or in combination with RSPO3. Thus, these data show that Wnt signaling can synergize with FGF19 signaling to induce a rapid increase in liver size.

TaqMan analysis on liver and ileum of treated mice showed that both Fgf15 and FGF19 repressed *Cyp7a1* expression in liver and Fgf15 expression in ileum (via reduction in circulating BAs) as single agents and in combination with RSPO3 (Figure 3B). The reduction in *Cyp7a1* mRNA expression was consistent with decreased Cyp7a1 protein observed in liver sections (Figure 3C). Expression of Zone 3 marker glutamine synthetase was expanded in RSPO3-treated livers, with or without expression of Fgf15/FGF19, indicating that Wnt signaling is elevated in these livers (Figure 3C). Thus, even in the context of Wnt activation, Fgf15 and FGF19 can repress *Cyp7a1* expression and inhibit production of BAs.

In addition to changes in liver size and gene expression, we observed two remarkable metabolic changes in serum chemistry of mice treated with RSPO3 + FGF19: blockade of fasting-induced ketogenesis and elevated cholesterol levels (Figure 3D). Upon fasting, the liver normally upregulates ketogenesis to compensate for the lack of feeding. While RSPO3 alone potentiated fasting-induced ketogenesis (assessed by serum levels of the ketone body beta-hydroxybutyric acid), it was completely blocked in the presence of RSPO3 + FGF19, but not RSPO3 + Fgf15 (Figure 3D). We also observed a significant increase in total cholesterol in mice treated with RSPO3 + FGF19 under both fasted and fed conditions (Figure 3D) that cannot be attributed to inhibition of BA production. ALT/AST levels were normal in these mice, indicating that changes in serum chemistry are not due to toxicity or liver damage (Figure S6C). Together, our findings establish important differences in the biological functions of FGF19 and Fgf15, as Fgf15 is unable to cooperate with RSPO3 to induce liver growth or serum chemistry changes.

3.4 | Fgf15/19 monomers exhibit enhanced mitogenicity relative to dimeric forms in vivo

To test the ability of FGF19^{P128C} and Fgf15^{C135P} to synergize with RSPO3 to stimulate liver growth, RSPO3 alone or in

combination with wild-type or mutant proteins was expressed via HDD. Combined results from three independent experiments are shown in Figure 4A. While Fgf15 did not synergize with RSPO3 to induce liver growth, Fgf15^{C135P} was able to induce a modest, though not statistically significant, increase in liver weight relative to RSPO3 alone. FGF19^{P128C} was a less potent mitogen than wild-type FGF19 when combined with RSPO3, a difference that was statistically significant (Figure 4A). These data mirror what was observed in vitro with AML12 hepatocytes, that is, the mitogenic activity of FGF19 > FGF19^{P128C} and that of Fgf15^{C135P} > Fgf15. Thus, monomeric ligands are more potent mitogens in vivo than their dimeric counterparts.

The mutations to remove or introduce the unpaired cysteines also altered the effects of Fgf15/FGF19 on serum chemistry of mice. Compared to RSPO3 alone, the RSPO3 + FGF19 group exhibited higher cholesterol and reduced fasting-induced ketogenesis, effects that were less pronounced with FGF19^{P128C} (Figure 4B). Additionally, wild-type Fgf15 had no impact on ketogenesis or cholesterol in combination with RSPO3. However, monomeric Fgf15^{C135P} in combination with RSPO3 promoted a small increase in serum cholesterol (compared to RSPO3 alone) and modest inhibition of fasting-induced ketogenesis (Figure 4B). Wild-type and mutant constructs were all able to inhibit *Cyp7a1* and *Fgf15* expression (Figure S7).

Previous publications have shown that a variant of FGF19, dubbed M70, is unable to induce liver tumorigenesis when overexpressed in certain mouse strains.² While this variant was able to activate Erk phosphorylation, its failure to induce proliferation was attributed to an inability to induce Stat3 phosphorylation. To test if this variant is able to synergize with RSPO3 to induce liver growth, constructs encoding RSPO3 and FGF19 or M70 were delivered to SCID mice via HDD (Figure S8A) and liver weights measured 2 weeks later (Figure 4C). As shown in Figure 4C, M70 was able to induce liver growth in the presence of RSPO3 to the same extent as wild-type FGF19. In vitro, M70 had a modest effect on AML12 proliferation, less than that of FGF19 (Figure S8B). Additionally, FGF19 and M70 were equally able to stimulate phosphorylation of Erk and Plcg1 in vitro (Figure S8C). These data are consistent with a model in which the monomeric structure of Fgfr4 ligands is crucial to their function, and point to Erk phosphorylation as a key mediator of the ability to potentiate liver growth in the presence of active Wnt signaling.

3.5 | Il6/Stat3 signaling is not required for FGF19-driven liver growth in the presence of RSPO3

It has been reported that induction of hepatocyte proliferation and liver tumorigenesis by FGF19 involves a

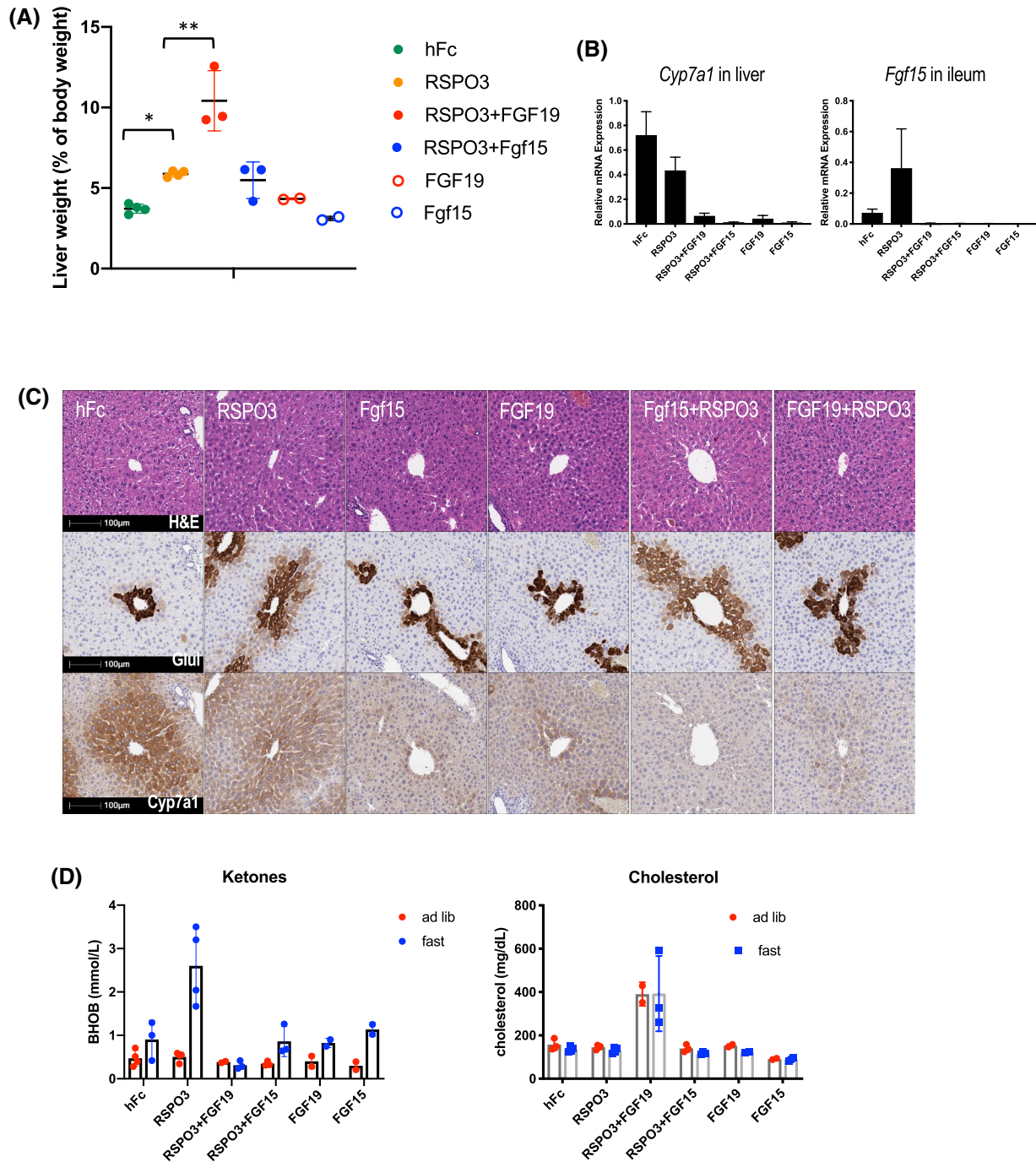


FIGURE 3 FGF19 can synergize with RSPO3 to induce hepatomegaly. A, Liver to body weight ratio from male mice 2 weeks post-HDD with 50 µg/mouse (25 µg/mouse for FGF single treatment) of plasmid encoding the indicated proteins, fasted for 18h before sacrifice. (* $P < .05$; ** $P < .005$ using ANOVA with Tukey's multiple comparisons test). B, Mice from A. mRNA levels of *Cyp7a1* (liver) or *Fgf15* (ileum) from male mice at 1 week post-HDD. Bar graph depicts the relative mRNA levels vs the empty vector control group (assigned a value of 1.0). Mean \pm standard deviation, $n = 4$ for control and RSPO3; $n = 3$ for RSPO3 + FGF19, RSPO3 + FGF15; and $n = 2$ for FGF19 and FGF15. PCR reactions done in triplicate, normalized to beta-actin. C, Mice from A. Livers sections stained with hematoxylin and eosin (H&E) or antibodies against glutamine synthetase (Glut) or Cyp7a1. Images are centered on the pericentral region. D, β -hydroxybutyrate and total cholesterol serum levels in mice from A and a matched group fed ad lib. Bar graphs depicts mean \pm standard deviation. $n = 4$ hFc fasted, RSPO3 ad lib, fasted; $n = 3$ hFc ad lib, RSPO3 + FGF19 fasted; RSPO3 + Fgf15 ad lib, fasted; and $n = 2$ RSPO3 + FGF19 ad lib, FGF19 ad lib, fasted, RSPO3 + Fgf15 ad lib, fasted. Each sample measured in duplicate. Data from one of four representative experiments in male and female mice are graphed.

non-cell-autonomous mechanism in which FGF19 induces innate immune cells to produce IL6 (mechanism unknown), which in turn activates Stat3 in hepatocytes.⁷ To test if IL6

signaling is required for FGF19 synergy with RSPO3 to induce liver growth in our system, we utilized an in-house IL6 receptor (IL6r) antibody known to block ligand binding and

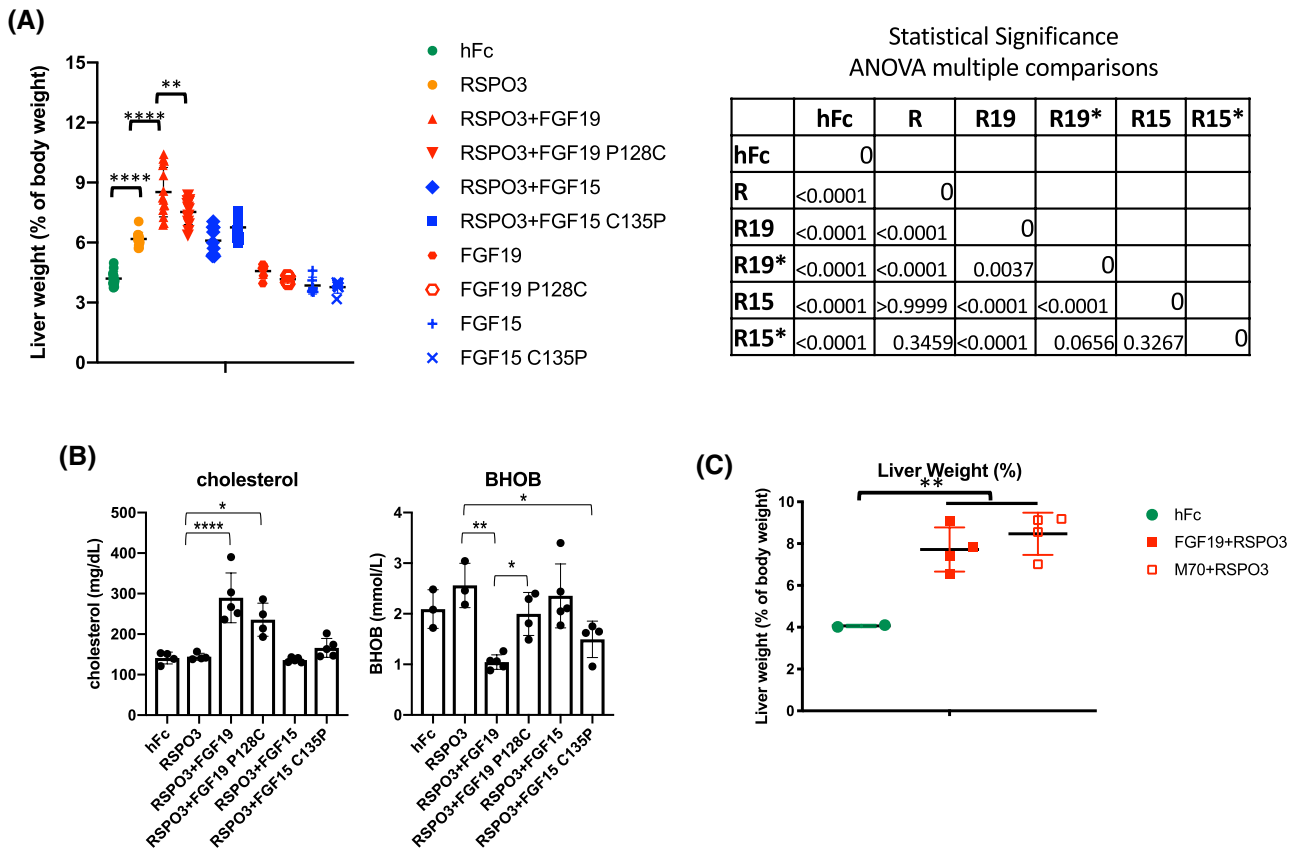


FIGURE 4 Alterations in structure modulate the ability of Fgf15/FGF19 to synergize with RSPO3 to induce hepatomegaly. A, Liver to body weight ratios of male mice at 2 weeks post-HDD with 50 μ g/mouse (25 μ g/mouse for FGF single treatment) of plasmid encoding the indicated proteins, fasted for 18 hours. hFc n = 13, RSPO3 n = 14, RSPO3 + FGF19 n = 14, RSPO3 + FGF19^{P128C} n = 14, RSPO3 + FGF15 n = 9, RSPO3 + FGF15^{C135P} n = 13, FGF19 n = 6, FGF19^{P128C} n = 6, FGF15 n = 6, and FGF15^{C135P} n = 6. (** P < .005; **** P < .0001 using ANOVA with Tukey's multiple comparisons test. All comparisons in chart.) B, β -hydroxybutyrate and total cholesterol serum levels in a subset of mice from A. Graphs depict mean \pm standard deviation. n = 3 hFc and RSPO3, n = 4 RSPO3 + FGF19^{P128C} and RSPO3 + Fgf15^{C135P}, and n = 5 RSPO3 + FGF19 and RSPO3 + Fgf15. * P < .05, ** P < .005; **** P < .0001 using ANOVA with Tukey's multiple comparisons test. C, Liver to body weight ratios of male mice at 2 weeks post-HDD with 50 μ g/mouse (25 μ g/mouse for FGF single treatment) of plasmid encoding the indicated proteins, fasted for 18 hours. hFc n = 2, FGF19 n = 4, M70 n = 4, ** P < .005 using ANOVA with Tukey's multiple comparisons test.

downstream Il6r signaling. Mice were dosed with 25 mg/kg of control antibody or Il6r blocking antibody 24 hours prior to HDD with plasmids encoding RSPO3 and the various Fgf15/FGF19 proteins. As shown in Figure 5A, Il6r blockade did not prevent FGF19 from potentiating the effect of RSPO3 on liver size (nor did Il6r blockade inhibit RSPO3-induced liver growth). Il6r blockade also had no impact on *Cyp7a1* repression by FGF19 (Figure 5C). HDD with plasmids encoding *FGF19* or *Il6* in combination with control or Il6r blocking antibody treatment showed that while the Il6r antibody had no impact on FGF19-induced Stat3 phosphorylation, it did block Il6-induced Stat3 phosphorylation, confirming antibody efficacy in vivo (Figure 5B). These data indicate that FGF19 does not require Il6 to induce liver growth in the presence of RSPO3 and is consistent with a model whereby the effects of FGF19 on proliferation are attributable to the direct activation of mitogenic signaling pathways such as Plcg1 and Erk.

4 | DISCUSSION

We have shown here that FGF19 is a more potent activator of Fgfr4/Klb signaling than its ortholog, Fgf15, due to the presence of an unpaired cysteine in Fgf15 that is necessary and sufficient for dimerization. Furthermore, disulfide-linked homodimers of wild-type Fgf15 and FGF19^{P128C} are less effective ligands than their monomeric counterparts. We did not find any evidence that qualitative differences in downstream pathway activation result from monomeric vs dimeric structure. Thus, the primary difference between orthologs Fgf15 and FGF19 is not which signaling pathways they activate, but the potency with which these pathways are activated. Potency is determined, at least in part, by ligand conformation. Interestingly, ligand conformation did not alter the ability of the FGFs to inhibit expression of *Cyp7a1* in vivo, implying that weak activation of Fgfr4/Klb is sufficient to fully repress the *Cyp7a1* promoter.

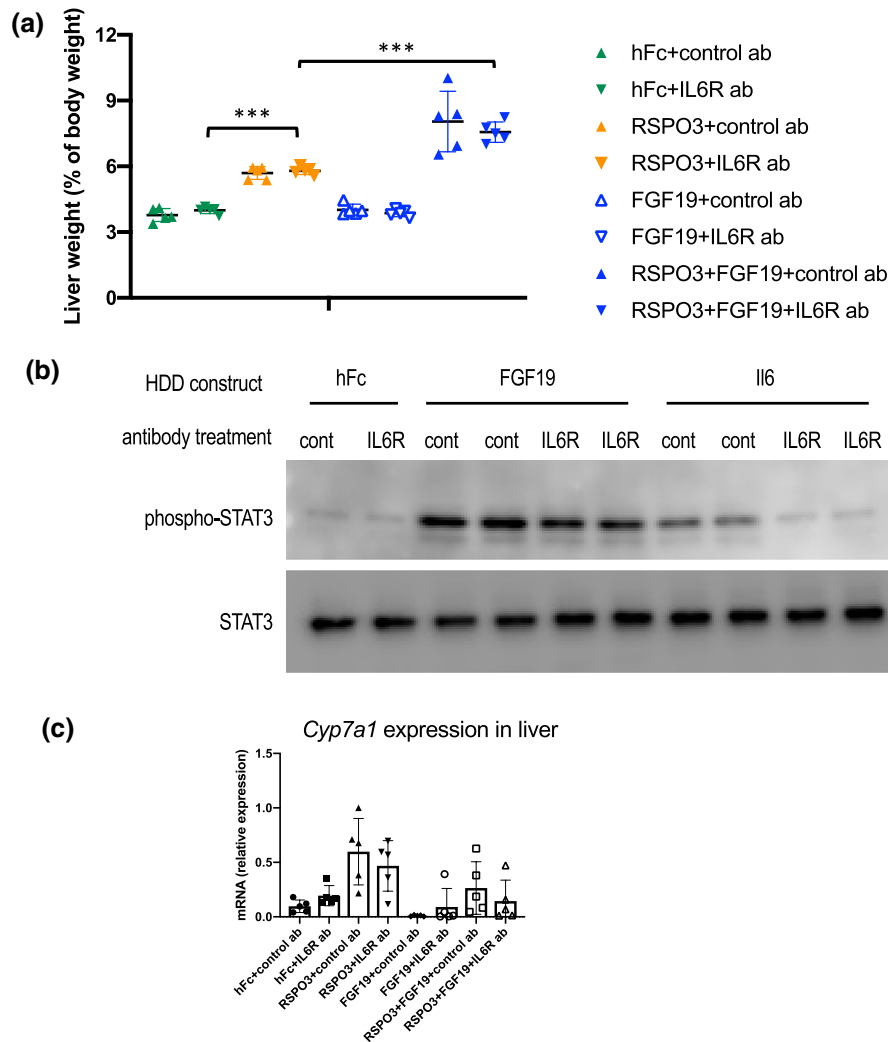


FIGURE 5 IL6/Stat3 axis does not control FGF19-driven liver growth in the presence of RSPO3. A, Liver to body weight ratios at 2 weeks post-HDD of male mice treated with control or IL6R blocking antibody dosed at 25 mg/kg 1 day prior to HDD and twice per week thereafter, fasted 18 hours before sacrifice. $n = 5$ mice per group, $**P < .005$ using ANOVA with Tukey's multiple comparisons test. B, Western blot of liver lysates from male mice 5 days post-HDD with 50 $\mu\text{g}/\text{mouse}$ of plasmid encoding FGF19 or 0.5 $\mu\text{g}/\text{mouse}$ of plasmid encoding IL6, dosed with control antibody (cont) or IL6R blocking antibody (IL6R) at 25 mg/kg. C, Mice from A. Bar graph depicts relative *Cyp7a1* (liver) and *Fgf15* (ileum) mRNA levels vs the empty vector control group (assigned a value of 1.0). Mean \pm standard deviation. $n = 5$, PCR reactions done in triplicate, normalized to beta-actin.

One limitation of this study is the inability to distinguish between a model in which only monomeric Fgf15/FGF19 signal and one in which dimeric ligands can signal, but with reduced potency. It appears that a small proportion of wild-type Fgf15 may exist as a monomer, since weak bands of monomeric Fgf15 are visible on non-reducing gels from conditioned media and mouse sera. This small fraction of monomer may be sufficient to inhibit *Cyp7a1* expression in vivo, but insufficient to drive mitogenic signaling. Alternatively, dimeric Fgf15/FGF19 may be able to bind and signal via Fgfr4/Klb, but less effectively due to allosteric differences that limit Fgfr4 dimerization and phosphorylation. An X-ray crystal structure of Fgfr4/Klb in complex with Fgf15 or FGF19 would help to clarify these issues. Regardless of which model is true, our data demonstrate that Fgf15 and

FGF19 are markedly different in their signaling strength. Of note, studies that have used recombinant FGF19 to investigate effects on signaling or proliferation in vitro have often stated that the findings apply to both Fgf15/FGF19, a conclusion that is unlikely to be valid.^{9,21}

FGF19 and Wnt play well-established roles in liver regeneration and control of liver size, but cooperation between the two pathways has not been previously appreciated. Wnt enhancer RSPO3 was able to induce a rapid and stable increase in liver size within 2 weeks of HDD and FGF19 was able to enhance this effect, resulting in a doubling of liver size. Remarkably, the liver growth induced by both RSPO3 and RSPO3 + FGF19 is controlled, rapid, and stable for up to 6 months in SCID mice (Figure S9). This stable liver size, where growth plateaus and is maintained even if mice are re-dosed via HDD, indicates that

we are not inducing uncontrolled liver growth, but instead a specific program of the hepatostat. We have not ruled out the possibility that HDD itself triggers a regenerative response, as control HDD does induce transient hepatocyte proliferation which resolves by 1 week without an increase in liver size (data not shown). However, since redosing the mice does not further enlarge the livers, RSPO3 and FGF19 likely converge on the hepatostat and do not merely boost regeneration.

This phenomenon of FGF19 enhancing Wnt-induced mitogenicity in vivo may be relevant to therapeutic settings where FGFR4/KLB signaling is being activated in the presence of ongoing Wnt signaling. The FGF19 variant M70 (NGM282/aldefermin) is currently showing promise in treatment of primary sclerosing cholangitis (PSC).¹⁵ RSPO3 may be a crucial modulator of PSC-associated scarring necessitating liver transplant,²² but the role of Wnt signaling is not completely understood.²³ NGM282 is also showing promise in alleviating NASH-associated fibrosis,¹⁴ another process where Wnt signaling²⁴ and RSPO3 in particular are implicated.²⁵ In our model, M70 was able to induce liver growth in combination with RSPO3 to the same extent as wild-type FGF19 (Figure 4C), despite being reported not to induce hepatocyte proliferation as a single agent. M70 has been shown to stimulate Erk phosphorylation to the same extent as FGF19 in vivo⁶ and our data show that the extent of Erk activation is a key difference between Fgf15 and FGF19 signaling downstream of Fgfr4. The ability of M70 to activate Erk may account for its ability to synergize with RSPO3 to induce liver growth and to modestly promote hepatocyte proliferation in vitro (Figure S6C). Thus, preclinical data suggest that the use of M70/NGM282 in settings where Wnt signaling is likely to be active could potentially result in hepatocyte proliferation, and may warrant monitoring.

FGF19 is amplified in a subset of HCC and recent clinical data confirm its status as a cancer driver.^{8,11,26} However, efforts to inhibit the FGF19/FGFR4/KLB signaling axis have been limited by BA-induced toxicity. On target toxicity in the gut and liver have halted development of FGF19 and FGFR4 blocking antibodies,¹⁰ and FGFR4 small molecule inhibitors have shown significant on-target toxicities.¹¹ Thus, an optimal therapeutic agent might be an FGFR4 antibody that blocks FGF19 binding (thereby inhibiting the oncogenic signal) while at the same time acting as a weak agonist, that is, repressing *CYP7A1* expression but not stimulating key mitogenic pathways like ERK. M70/NGM282 is non-oncogenic in mouse models. However, in our studies, M70/NGM282-induced liver growth in the presence of RSPO3 to the same extent as wild-type FGF19. Furthermore, it is uncertain whether the ability of M70/NGM282 to activate ERK would be a liability in the HCC setting. An alternative could be to use FGF19^{P128C} (following purification of the dimeric species and assuming that dimeric ligands can signal weakly), which does not cooperate with RSPO3 to induce liver growth but retains the ability to repress *Cyp7a1* expression.

In summary, we show here that Fgf15/FGF19 structure and function are intricately linked and that ligand conformation controls signaling strength. A better mechanistic understanding of how Fgf15 and FGF19 signaling differ could help inform strategies to target this pathway, with the goal of maintaining metabolic signaling while inhibiting mitogenic signaling in diseases such as HCC and NASH.

ACKNOWLEDGMENTS

The authors thank the Regeneron Animal Facility, the Tissue Culture Core, the Serum Chemistry Core, and the DNA Core at Regeneron.

CONFLICT OF INTEREST

The authors declare no conflict of interest.

AUTHOR CONTRIBUTIONS

C.M. Williams, C. Daly, M. Carbonaro, Z. Li, and G. Thurston designed the research; C.M. Williams and M.P. Molina-Portela analyzed and interpreted the data; J. Harper Calderon, H.E. Tan, Y. Jimenez, K. Berringer, and M. Carbonaro performed the research; C.M. Williams, J. Harper Calderon, M. Carbonaro, M.P. Molina-Portela, G. Thurston, Z. Li, and C. Daly wrote and reviewed the manuscript.

ORCID

Courtney M. Williams  <https://orcid.org/0000-0001-8618-8320>

REFERENCES

- Wright TJ, Ladher R, McWhirter J, Murre C, Schoenwolf GC, Mansour SL. Mouse FGF15 is the ortholog of human and chick FGF19, but is not uniquely required for otic induction. *Dev Biol.* 2004;269:264-275.
- Zhou M, Luo J, Chen M, et al. Mouse species-specific control of hepatocarcinogenesis and metabolism by FGF19/FGF15. *J Hepatol.* 2017;66:1182-1192.
- Kong B, Huang J, Zhu Y, et al. Fibroblast growth factor 15 deficiency impairs liver regeneration in mice. *Am J Physiol Gastrointest Liver Physiol.* 2014;306:G893-G902.
- Xie MH, Holcomb I, Deuel B, et al. FGF-19, a novel fibroblast growth factor with unique specificity for FGFR4. *Cytokine.* 1999;11:729-735.
- Nicholes K, Guillet S, Tomlinson E, et al. A mouse model of hepatocellular carcinoma: ectopic expression of fibroblast growth factor 19 in skeletal muscle of transgenic mice. *Am J Pathol.* 2002;160:2295-2307.
- Zhou M, Wang X, Phung V, et al. Separating tumorigenicity from bile acid regulatory activity for endocrine hormone FGF19. *Cancer Res.* 2014;74:3306-3316.
- Zhou M, Yang H, Learned RM, Tian H, Ling L. Non-cell-autonomous activation of IL-6/STAT3 signaling mediates FGF19-driven hepatocarcinogenesis. *Nat Commun.* 2017;8:15433.
- Sawey ET, Chanrion M, Cai C, et al. Identification of a therapeutic strategy targeting amplified FGF19 in liver cancer by oncogenomic screening. *Cancer Cell.* 2011;19:347-358.

9. Uriarte I, Latasa MU, Carotti S, et al. Ileal FGF15 contributes to fibrosis-associated hepatocellular carcinoma development. *Int J Cancer*. 2015;136:2469-2475.
10. Pai R, French D, Ma N, et al. Antibody-mediated inhibition of fibroblast growth factor 19 results in increased bile acids synthesis and ileal malabsorption of bile acids in cynomolgus monkeys. *Toxicol Sci*. 2012;126:446-456.
11. Kim RD, Sarker D, Meyer T, et al. First-in-human phase I study of fisogatinib (BLU-554) validates aberrant FGF19 signaling as a driver event in hepatocellular carcinoma. *Cancer Discov*. 2019;9:1696-1707.
12. Zhou M, Learned RM, Rossi SJ, DePaoli AM, Tian H, Ling L. Engineered FGF19 eliminates bile acid toxicity and lipotoxicity leading to resolution of steatohepatitis and fibrosis in mice. *Hepatol Commun*. 2017;1:1024-1042.
13. Harrison SA, Rinella ME, Abdelmalek MF, et al. NGM282 for treatment of non-alcoholic steatohepatitis: a multicentre, randomised, double-blind, placebo-controlled, phase 2 trial. *Lancet*. 2018;391:1174-1185.
14. Harrison SA, Rossi SJ, Paredes AH, et al. NGM282 improves liver fibrosis and histology in 12 weeks in patients with nonalcoholic steatohepatitis. *Hepatology*. 2020;71:1198-1212.
15. Hirschfield GM, Chazouilleres O, Drenth JP, et al. Effect of NGM282, an FGF19 analogue, in primary sclerosing cholangitis: a multicenter, randomized, double-blind, placebo-controlled phase II trial. *J Hepatol*. 2019;70:483-493.
16. Mayo MJ, Wigg AJ, Leggett BA, et al. NGM282 for treatment of patients with primary biliary cholangitis: a multicenter, randomized, double-blind, placebo-controlled trial. *Hepatol Commun*. 2018;2:1037-1050.
17. Liu F, Song Y, Liu D. Hydrodynamics-based transfection in animals by systemic administration of plasmid DNA. *Gene Ther*. 1999;6:1258-1266.
18. Wu JC, Merlino G, Fausto N. Establishment and characterization of differentiated, nontransformed hepatocyte cell lines derived from mice transgenic for transforming growth factor alpha. *Proc Natl Acad Sci U S A*. 1994;91:674-678.
19. Hammad S, Hoehme S, Friebe A, et al. Protocols for staining of bile canalicular and sinusoidal networks of human, mouse and pig livers, three-dimensional reconstruction and quantification of tissue microarchitecture by image processing and analysis. *Arch Toxicol*. 2014;88:1161-1183.
20. Naugler WE, Tarlow BD, Fedorov LM, et al. Fibroblast growth factor signaling controls liver size in mice with humanized livers. *Gastroenterology*. 2015;149:728-740.e15.
21. Li Q, Zhao Q, Zhang C, et al. The ileal FGF15/19 to hepatic FGFR4 axis regulates liver regeneration after partial hepatectomy in mice. *J Physiol Biochem*. 2018;74:247-260.
22. Alberts R, de Vries EMG, Goode EC, et al. Genetic association analysis identifies variants associated with disease progression in primary sclerosing cholangitis. *Gut*. 2018;67:1517-1524.
23. Wilson DH, Jarman EJ, Mellin RP, et al. Non-canonical Wnt signalling regulates scarring in biliary disease via the planar cell polarity receptors. *Nat Commun*. 2020;11:445-457.
24. Nishikawa K, Osawa Y, Kimura K. Wnt/beta-Catenin signaling as a potential target for the treatment of liver cirrhosis using antifibrotic drugs. *Int J Mol Sci*. 2018;19:3103-3114.
25. Zhang M, Haughey M, Wang NY, et al. Targeting the Wnt signaling pathway through R-spondin 3 identifies an anti-fibrosis treatment strategy for multiple organs. *PLoS ONE*. 2020;15:e0229445.
26. Kaibori M, Sakai K, Ishizaki M, et al. Increased FGF19 copy number is frequently detected in hepatocellular carcinoma with a complete response after sorafenib treatment. *Oncotarget*. 2016;7:49091-49098.

SUPPORTING INFORMATION

Additional Supporting Information may be found online in the Supporting Information section.

How to cite this article: Williams CM, Harper Calderon J, E H, et al. Monomeric/dimeric forms of Fgf15/FGF19 show differential activity in hepatocyte proliferation and metabolic function. *The FASEB Journal*. 2021;35:e21286. <https://doi.org/10.1096/fj.202002203R>